

DOI: 10.1002/adma.200501077

Conformally Back-Filled, Non-close-packed Inverse-Opal Photonic Crystals**

By Jeffrey S. King, Davy P. Gaillot, Elton Graugnard, and Christopher J. Summers*

Photonic crystals (PCs) offer far greater control over the generation and propagation of light than any other material structures.^[1,2] Their defining characteristics, omnidirectional and directional photonic bandgaps (PBGs), can be manipulated to enable effects such as low losses in optical circuits and control of spontaneous emission. PCs are also creating much excitement because of their ability to form flat bands, yielding phenomena such as slow light and negative refraction.^[3,4] The infiltration and inversion of synthetic-opal templates has been established as a promising method for obtaining the periodic structure and refractive-index contrast required in PCs.^[5–9] In addition, topological tuning by shifting the distribution and filling fraction of a high-dielectric material within PCs offers a way to significantly change their photonic-band properties. For example, increased tunability, functionality, and bandgap properties can be accomplished through advanced architectures such as multilayered inverse opals and non-close-packed (NCP) inverse opals.^[10–13] NCP geometries differ significantly from inverse opals by the formation of extended “air cylinders” between neighboring air spheres, as shown in Figure 1a, whereas, in the more-limited inverse opal, the air spheres are connected only by narrow “sinter necks.” As reported by Doosje et al., silicon NCP architectures are predicted to yield a 100 % increase in the width of the omnidirectional PBG between the eighth and ninth photonic bands.^[12]

In this paper, we show that modification of PC-template topology by both heat treatment and multiple conformal infiltrations facilitates precise control and optimization of photonic-band properties. Static tuning is possible by precisely controlled backfilling of inverse opals to increase the filling fraction of dielectric material.^[14] However, inverse opals have inherently limited filling-fraction tunability because the narrow sinter necks quickly close with backfilling. To solve this limitation, we report the implementation of a new, two-step atomic layer deposition (ALD) infiltration process to form a

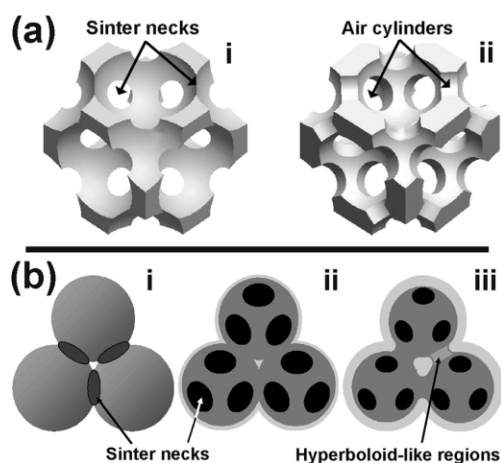


Figure 1. a) Dielectric distribution in i) close-packed and ii) NCP inverse opals. Note cylindrical connections (air cylinders) between air spheres labeled in (ii), and “sinter” necks labeled in (i). b) NCP inverse-opal fabrication route: i) heavily sintered opal template, ii) resulting inverse opal, and iii) NCP inverse opal after atomic layer deposition backfilling.

TiO₂ NCP inverse opal. Significantly, this new process allowed a static tunability of ~400 nm in the position of the directional bandgap. In the first step, the void space available for infiltration was reduced to ~25 % of the original volume by controllably collapsing the opal template by sintering followed by ALD infiltration, a method that is capable of high-finesse deposition of dense films within a nanoporous template. This facilitated the formation of an ultralow-filling-fraction inverse opal (5.8 %) with 193 nm diameter sinter necks. In the second step, backfilling of the low-volume-fraction inverse opal resulted in large tuning of the photonic-band properties and, ultimately, the formation of an NCP structure. Because of its many applications in biosensing, solar cells, catalysis, and environmental cleanup, optically active and tunable TiO₂ structures are of high interest.

In this study, silica opal templates were first grown on silicon substrates in a manner similar to that of Park and co-workers, as described elsewhere.^[15,16] The steps that were next taken to form an NCP inverse opal are illustrated in Figure 1b. First, a 10 μm thick opal template with 460 nm sphere diameter was sintered at 1000 °C for 3 h (Fig. 1b, step i), which is considerably longer and at a higher temperature than the “normal” sintering condition of 800 °C for 2 h, in order to partially collapse the template and increase the sinter-neck diameter. TiO₂ was then conformally deposited in the very small air voids (<10 nm) using ALD, a technique that has re-

[*] Prof. C. J. Summers, Dr. J. S. King,^[†] D. P. Gaillot, Dr. E. Graugnard
School of Materials Science and Engineering
Georgia Institute of Technology
771 Ferst Drive, Atlanta, GA 30332-0245 (USA)
E-mail: chris.summers@mse.gatech.edu

[†] Present address: Department of Chemical Engineering, Stanford University, 381 North–South Mall, Stanford, CA 94305-5025, USA.

[**] This work was supported by the U.S. Army Research Office contract DAAD19-01-1-0603.

cently shown high potential for PC fabrication.^[11,16–20] The ability of ALD to fully and homogeneously infiltrate nanoporous structures was critical to achieving uniform infiltration of the narrow air channels (approximately four times smaller than conventional opals) of the sintered opal. The infiltrated sample was next heated to 400 °C and held for 2 h to convert the as-deposited amorphous TiO₂ to the anatase phase. The top surface was then removed using an ion mill to expose the silica template, and etching in a 2 % HF solution resulted in the complete removal of the spheres. This first stage resulted in the formation of an ultralow filling fraction (~5.8 vol.-%), structurally stable inverse opal, with a ~220 % greater sinter neck diameter than possible in a typical inverse opal (Fig. 1b, step ii).

In the second stage of the experiment, the TiO₂ PC's structure and optical properties were precisely tuned by backfilling the modified inverse-opal template with increasing TiO₂ depositions. The conformal nature of ALD allowed the periodicity of the inverse opal to be maintained, even for high levels of backfilling. Furthermore, the large sinter-neck diameter permitted significant backfilling, resulting in the formation of cylindrical (or hyperboloid-like) connections between the air spheres, thus yielding a well-formed NCP inverse opal, as shown in Figure 1b, step iii. This conformal model differs from that of Figure 1a, panel ii, a “geometrical” model, which is the same as the dielectric function used for band calculations by Doosje et al.^[12] and Fenollosa and Meseguer.^[13]

Figure 2 shows cross-sectional scanning electron microscopy (SEM) images through the (111) plane of the NCP inverse

opals. A schematic of the predicted 2D geometry of the air regions for each step is superimposed on the left of the images. The inverse opal produced by infiltration of a heavily sintered ~460 nm opal followed by HF etching is shown in Figure 2a. As expected, the overall lattice constant was reduced, and measurement of the periodicity of the structure in the image revealed a 400 nm spacing between repeat units in the (111) plane. The resulting air-sphere diameter was ~415 nm, slightly larger than the periodicity, but less than the original sphere size of 460 nm. Most significantly, the image indicates a 193 nm average diameter of the sinter necks, indicating formation of large pathways for gas flow within the structure. This structure is superior to a “normal” inverse opal because it increased by 220 % the amount of backfilling possible before the pores closed, improving the static tunability of the PC. After backfilling with 240 ALD cycles, the structure in Figure 2b was formed, in which the air spheres and sinter necks have been significantly reduced in diameter, and hyperboloid-like inter-sphere connections have formed. The air-sphere and hyperboloid (sinter neck) radii decreased further after backfilling with an additional 320 ALD cycles (Figs. 2c and d). The formation of hyperboloid necks, air-sphere size tuning, and change in TiO₂ filling fraction, while maintaining a constant lattice constant, dramatically shows the degree of PC structural tuning achievable with this technique.

To probe the resulting photonic-band structures in the Γ -L direction, specular reflectivity at 15° incidence to the (111) planes was measured during each processing step of the NCP

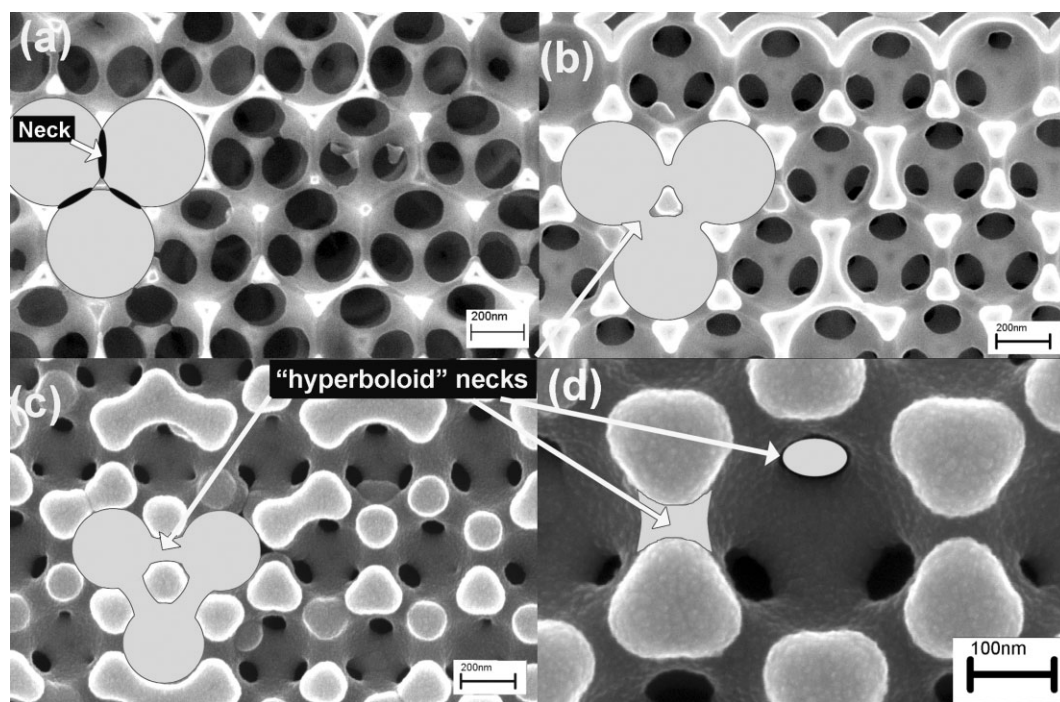


Figure 2. SEM images of ion-milled cross sections of the (111) plane of a) a TiO₂ inverse opal, formed from a heavily sintered 460 nm SiO₂ opal, b,c) an NCP inverse opal formed after 240 (b) and 560 (c) TiO₂ ALD backfilling cycles, and d) a higher-magnification image of the structure in (c). In (a), the dark shaded region indicates air-sphere overlap, as illustrated by the presence of large sinter necks. In (b,c,d), dark shaded regions highlight formation of hyperboloid-shaped connections between the air spheres of the new structure.

inverse opal. Figure 3a, curve i shows the spectrum of the heavily sintered opal, with a sharp, symmetrical Bragg reflectivity peak at 885 nm, and a sharp, lower-intensity peak at ~440 nm attributed to flat band effects. As discussed by Miquez et al.^[21] and Galisteo-López and López,^[22] face-cen-

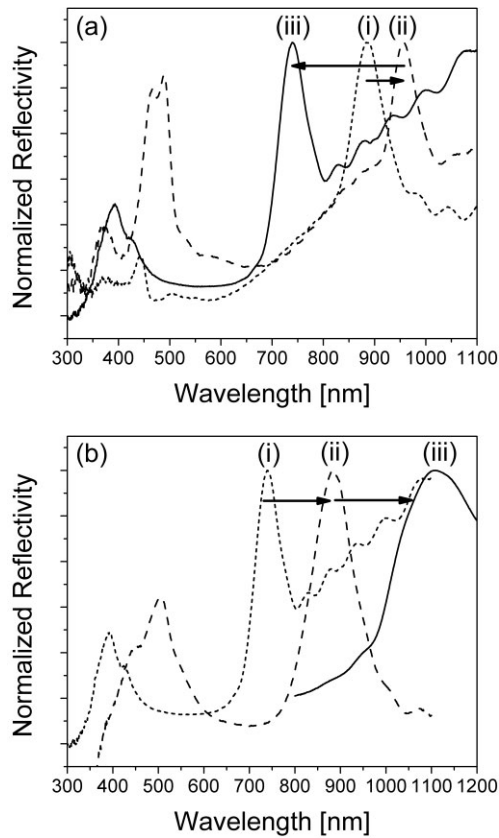


Figure 3. Reflectivity spectra for a) the first stage of fabrication: i) a heavily sintered SiO₂ opal, ii) a heavily sintered SiO₂ opal infiltrated with 340 cycles (~17 nm) of TiO₂, and iii) an inverse NCP opal with 400 nm (111) periodicity and 5.8% TiO₂ filling fraction. b) For the second stage of fabrication: i) a 5.8% filling fraction inverse NCP opal, and after infiltration with b) 240 ALD cycles (~12 nm) of TiO₂ and c) 640 ALD cycles (~33 nm). (Specular reflectivity with a 15° incidence was measured).

tered-cubic opals (and their derivatives) show reflectivity peaks not only in the presence of a bandgap, but also when the bands flatten. At these points, the group velocity slows, resulting in an increase in the refractive index and a resultant increase in reflectivity. After complete infiltration (Fig. 3a, curve ii), the peak remained sharp and symmetrical and shifted to 955 nm, which is much less than typically observed for infiltration of a conventional opal due to the reduced available air void volume. The flat band peak shifted to ~475 nm and increased in intensity, close to that of the Bragg peak. After removing the SiO₂ spheres (Fig. 3a, curve iii), the Bragg peak remained sharp and well defined, and shifted to 739 nm, indicating a TiO₂ filling fraction of 5.8% (calculated from the Bragg optical diffraction equation). Two higher-order peaks were also present at 392 and 427 nm. This data

showed that, by careful heavy sintering, not only the pore volume could be reduced by a factor of four, resulting in a 3D network of ~10 nm pores, but also that conformal ALD can be used to achieve high-finesse template geometries. Remarkably, even with such a low filling fraction, the inverse opal was structurally stable, indicating a high TiO₂ density. This inverse-opal template was next infiltrated with amorphous TiO₂ in steps of 40 ALD cycles. Figure 3b shows the extremely wide range of tuning achievable after backfilling with 240 and 640 ALD cycles. A shift in the directional bandgap of 370 nm was realized, all from the same sample. Comparison of the evolution of the reflectivity spectra during the continual tuning of this NCP structure with the positions of the calculated (111) direction (Γ -L) fundamental bandgaps (Bragg peak) is shown in Figure 4a.

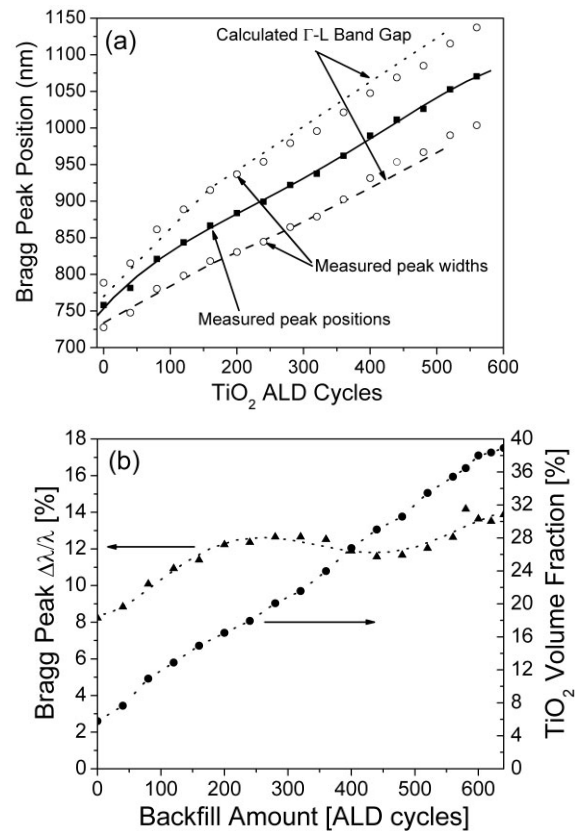


Figure 4. a) Comparison of peak positions (dark squares) and widths (open circles) ($\Delta\lambda/\lambda$) measured from reflectivity spectra with calculated positions of the second and third photonic bands (dotted lines) for the (111) (Γ -L) direction, and b) measured relative peak widths and TiO₂ volume fractions for a TiO₂ NCP inverse opal as a function of ALD backfilling.

Figure 4a shows the position of the calculated Γ -L directional bandgaps (dotted lines) and the measured Bragg-peak positions (solid circles) and widths (hollow circles).^[23] Both the peak positions and widths matched the predicted bandgap positions very well. The Bragg-peak $\Delta\lambda/\lambda$ ratios were calculated from the measured reflectivity spectra after each infil-

tration step by division of the full width at half maximum (FWHM) of the peak by its wavelength. The $\Delta\lambda/\lambda$ ratio is a reliable indicator of changes in the PBG width. Secondary contributions to peak width, such as disorder and sphere polydispersity, are not expected to impact the tuning shown in this work since the highly conformal nature of the ALD process does not introduce additional disorder. Thus, the intrinsic peak broadening will remain constant after the sintering step. The relative peak widths ($\Delta\lambda/\lambda$) as a function of ALD cycles and the corresponding filling fractions are shown in Figure 4b. As shown in the bottom curve, the filling fraction increased linearly with ALD cycles until the last 60–80 cycles. In this region, a decrease in the slope of the filling-fraction curve indicated that the cylinders had closed, and further infiltration was not possible. The top curve shows that the peak width clearly displayed a maximum of 12.7 % at approximately 280–320 ALD cycles (~20 % TiO₂ filling fraction), after which it decreased slightly to 11.6 %. However, after 440 ALD cycles (ca. 27 % TiO₂ filling fraction), the peak width increased with successive cycles, reaching a value of 14 % for the sample backfilled with 580 TiO₂ ALD cycles (36 % filling fraction). Additional infiltrations up to 640 ALD cycles (~36 nm) and a 39 % filling fraction yielded a subsequent decrease in peak width and diminished gains in the TiO₂ filling fraction.

In summary, a two-step ALD process was used to form non-close-packed inverse opals by 1) conformally infiltrating heavily sintered silica opals with TiO₂ and etching the spheres with hydrofluoric acid, and 2) conformally backfilling the resulting inverse opal. Extensive sintering of the silica-opal template increased the sinter-neck diameter by 220 % due to sphere coalescence, with a consequent fourfold decrease in the available internal pore size and volume. These results demonstrate that ALD, a surface-limited, highly controllable growth technique, has the unique ability to fully and uniformly infiltrate porous structures, even within extended nanoscale channels (<10 nm), which is critical to successful infiltration and inversion of the template. The inverse opal that resulted from infiltration of this template had a very low TiO₂ filling fraction (5.8 %), was structurally stable, and more significantly, had approximately 193 nm diameter sinter-neck regions connecting the air spheres. This topological transformation was essential for achieving high levels of backfilling (39 %) of the inverse opal and successful formation of hyperboloid-like connections between the air spheres that comprise the inverse opal. A 70 % increase in the TiO₂ filling fraction was attained over that possible without heavy pre-sintering (23 %).^[17] The large range of TiO₂ volume fractions confirmed the wide variety of structures possible and the high degree of Bragg-peak tuning, which is nearly 400 nm wider than the entire visible spectral region, and larger than has ever been reported. These observations dramatically demonstrate the degree of structural changes achievable by this technique. This study is the first to demonstrate the power of a two-stage ALD process to uniquely enable the precise formation and tuning of complex PC structures. We expect this technique to be applicable to a broad range of PCs and to enable

precise control and optimization of parameters that are critical for tuning the photonic-bandgap properties and dispersion characteristics.

Experimental

Monodisperse silica colloids were formed using the Stöber method and dispersed in ultrapure deionized (DI) water [24]. Silica opals were next grown by forced sedimentation in a confinement cell [15]. After sintering the opal films in air at 1000 °C for 3 h, TiO₂ was grown within the opal in a custom-built flow-style hot-wall ALD reactor. Conformal growth was accomplished using alternating 8 s pulses of TiCl₄ and H₂O, each separated by a 20 s, 225 sccm N₂ purge, while maintaining the substrate at 100 °C. The vacuum level within the reactor was ~500 mTorr during pulses and 200 mTorr during purges (1 Torr ~133 Pa). The precursor gases, derived from room-temperature liquid sources, were introduced to a N₂ carrier gas using computer-controlled solenoid valves. Post-deposition heat treatment was performed at 400 °C in the ALD reactor with a constant N₂ flow of 225 sccm. The surface of the heat-treated infiltrated opal was next ion-milled for several minutes with a 4 keV Ar⁺ beam at 15° incidence. To remove the silica spheres, the milled sample was immersed in a 2 % HF solution for 1 h. The surface was next rinsed with DI water and dried in an oven at 110 °C. Backfilling of the inverse opal utilized the same ALD infiltration routine.

All SEM images were acquired using a LEO 1530 scanning electron microscope. Reflectivity measurements were performed using a Beckman DU640 spectrophotometer. Photonic-band diagrams were calculated using the finite-difference time-domain method. For the calculated band diagrams in Figure 4, an average refractive-index value (n) for visible wavelengths was used ($n_{\text{anatase}} = 2.65$, $n_{\text{amorphous}} = 2.45$ at 500 nm) [25,26]. When calculating the photonic-band structures reported in this paper, a “conformal” model was used for generation of the required dielectric functions, which exactly simulates the ALD growth topology. This produced a dielectric function that matches the real structures, taking into account the actual shapes of the air spheres and the connecting regions between them that result after conformal backfilling.

Received: May 25, 2005

Final version: October 24, 2005

Published online: March 22, 2006

- [1] S. John, *Phys. Rev. Lett.* **1987**, *58*, 2486.
- [2] E. Yablonovitch, *Phys. Rev. Lett.* **1987**, *58*, 2059.
- [3] K. Sakoda, *Optical Properties of Photonic Crystals*, Springer, New York **2001**.
- [4] C. M. Soukoulis, *Photonic Crystals and Light Localization in the 21st Century*, Kluwer Academic, Dordrecht, The Netherlands **2001**.
- [5] J. E. G. J. Wijnhoven, W. L. Vos, *Science* **1998**, *281*, 802.
- [6] H. M. Yates, W. R. Flavell, M. E. Pemble, N. P. Johnson, S. G. Romanov, C. M. Sotomayor-Torres, *J. Cryst. Growth* **1997**, *170*, 611.
- [7] S. G. Romanov, N. P. Johnson, A. V. Fokin, V. Y. Butko, H. M. Yates, M. E. Pemble, C. M. S. Torres, *Appl. Phys. Lett.* **1997**, *70*, 2091.
- [8] A. Blanco, E. Chomski, S. Grabtchak, M. Ibisate, S. John, S. W. Leonard, C. López, F. Meseguer, H. Míguez, J. P. Mondla, G. A. Ozin, O. Toader, H. M. van Driel, *Nature* **2000**, *405*, 437.
- [9] Y. A. Vlasov, X.-Z. Bo, J. C. Sturm, D. J. Norris, *Nature* **2001**, *414*, 289.
- [10] F. García-Santamaría, M. Ibisate, I. Rodríguez, F. Meseguer, C. López, *Adv. Mater.* **2003**, *15*, 788.
- [11] J. S. King, D. Heineman, E. Graugnard, C. J. Summers, *Appl. Surf. Sci.* **2005**, *244*, 511.

- [12] M. Doosje, B. J. Hoenders, J. Knoester, *J. Opt. Soc. Am. B* **2000**, *17*, 600.
- [13] R. Fenollosa, F. Meseguer, *Adv. Mater.* **2003**, *15*, 1282.
- [14] H. Míguez, N. Tétreault, S. M. Yang, V. Kitaev, G. A. Ozin, *Adv. Mater.* **2003**, *15*, 597.
- [15] S. H. Park, D. Qin, Y. Xia, *Adv. Mater.* **1998**, *10*, 1028.
- [16] J. S. King, C. W. Neff, C. J. Summers, W. Park, S. Blomquist, E. Forsythe, D. Morton, *Appl. Phys. Lett.* **2003**, *83*, 2566.
- [17] J. S. King, E. Graugnard, C. J. Summers, *Adv. Mater.* **2005**, *17*, 1010.
- [18] A. Rügge, J. S. Becker, R. G. Gordon, S. H. Tolbert, *Nano Lett.* **2003**, *3*, 1293.
- [19] J. S. King, C. W. Neff, S. Blomquist, E. Forsythe, D. Morton, C. J. Summers, *Phys. Status Solidi B* **2004**, *241*, 763.
- [20] M. Scharrer, X. Wu, A. Yamilov, H. Cao, R. P. H. Chang, *Appl. Phys. Lett.* **2005**, *86*, 1.
- [21] H. Míguez, V. Kitaev, G. A. Ozin, *Appl. Phys. Lett.* **2004**, *84*, 1239.
- [22] J. F. Galisteo-López, C. López, *Phys. Rev. B: Condens. Matter Mater. Phys.* **2004**, *70*, 035 108.
- [23] For comparison with the calculations, the measured peak positions and widths were converted to values expected for normal incidence by using the Bragg equation for optical diffraction.
- [24] W. Stöber, A. Fink, E. Bohn, *J. Colloid Interface Sci.* **1968**, *26*, 62.
- [25] *Handbook of Optical Constants of Solids* (Ed: E. D. Palik), Vols. 1–3, Academic, San Diego, CA **1998**.
- [26] D. Heineman, *M. S. Thesis*, Georgia Institute of Technology **2004**.